The EMBO Journal (2010) 29, 546–558 | © 2010 European Molecular Biology Organization | Some Rights Reserved 0261-4189/10
www.embojournal.org

THE EMBO JOURNAL

EMBO open

Endocytosis restricts *Arabidopsis* KNOLLE syntaxin to the cell division plane during late cytokinesis

Yohann Boutté[1,2,7], Márcia Frescatada-Rosa[1], Shuzhen Men[1,2,8], Cheung-Ming Chow[3,9], Kazuo Ebine[4], Anna Gustavsson[1], Lenore Johansson[5], Takashi Ueda[4], Ian Moore[3], Gerd Jürgens[6] and Markus Grebe[1,2,7,*]

[1]Department of Plant Physiology, Umeå Plant Science Centre (UPSC), Umeå University, Umeå, Sweden, [2]Department of Forest Genetics and Plant Physiology, UPSC, Swedish University of Agricultural Sciences, Umeå, Sweden, [3]Department of Plant Sciences, University of Oxford, South Parks Road, Oxford, UK, [4]Department of Biological Sciences, Graduate School of Science, University of Tokyo, Bunkyo-ku, Tokyo, Japan, [5]Electron Microscopy Platform, Chemical and Biological Centre, Umeå University, Umeå, Sweden and [6]Centre for Plant Molecular Biology (ZMBP), Department of Developmental Genetics, University of Tübingen, Tübingen, Germany

Cytokinesis represents the final stage of eukaryotic cell division during which the cytoplasm becomes partitioned between daughter cells. The process differs to some extent between animal and plant cells, but proteins of the syntaxin family mediate membrane fusion in the plane of cell division in diverse organisms. How syntaxin localization is kept in check remains elusive. Here, we report that localization of the *Arabidopsis* KNOLLE syntaxin in the plane of cell division is maintained by sterol-dependent endocytosis involving a clathrin- and DYNAMIN-RELATED PROTEIN1A-dependent mechanism. On genetic or pharmacological interference with endocytosis, KNOLLE mislocalizes to lateral plasma membranes after cell-plate fusion. Fluorescence-loss-in-photo-bleaching and fluorescence-recovery-after-photo-bleaching experiments reveal lateral diffusion of GFP-KNOLLE from the plane of division to lateral membranes. In an endocytosis-defective sterol biosynthesis mutant displaying lateral KNOLLE diffusion, KNOLLE secretory trafficking remains unaffected. Thus, restriction of lateral diffusion by endocytosis may serve to maintain specificity of syntaxin localization during late cytokinesis.

*Corresponding author. Department of Plant Physiology, Umeå Plant Science Centre, Umeå University, Umeå SE-90187, Sweden.
Tel.: +46 90 786 8237; Fax: +46 90 786 8165;
E-mail: markus.grebe@plantphys.umu.se
[7]Present address: Department of Plant Physiology, UPSC, Umeå University, Umeå SE-90 187, Sweden
[8]Present address: Department of Plant Biology and Ecology, College of Life Sciences, Nankai University, Tianjin 300071, China
[9]Present address: Department of Biology, Chinese University of Hong Kong, Shatin, New Territories, Hong Kong, China

Received: 9 June 2009; accepted: 6 November 2009; published online: 3 December 2009

The EMBO Journal (2010) **29,** 546–558. doi:10.1038/emboj.2009.363; Published online 3 December 2009
Subject Categories: membranes & transport; plant biology
Keywords: *Arabidopsis*; cytokinesis; endocytosis; KNOLLE syntaxin; sterols

Introduction

Animal, fungal and plant cells display differences between their main modes of somatic cytokinesis (Barr and Grüneberg, 2007). Animal cells, for example, constrict the plasma membrane (PM) through a contractile actin ring generating a cleavage furrow. When constriction has progressed, a microtubule-based structure, the midbody, is established in the centre of the cleavage furrow to support execution of the final steps of cytokinesis. These involve membrane fusion at the site of cell division that contributes to the abscission of the daughter cells (Low *et al*, 2003; Gromley *et al*, 2005; Barr and Grüneberg, 2007; Montagnac *et al*, 2008). Somatic cytokinesis in higher plants displays a centre-out mode of division (Samuels *et al*, 1995; Jürgens, 2005). From early telophase onward, the phragmoplast, a microtubule and actin-filament-based structure directs vesicle accumulation to the mid-plane of the cell (Samuels *et al*, 1995; Jürgens, 2005). Here, vesicles derived from the *trans*-Golgi, and possibly from endosomes, fuse to form the cell plate (Dhonukshe *et al*, 2006; Reichardt *et al*, 2007). Cell-plate formation progresses centrifugally until the plate fuses with the lateral PMs (Samuels *et al*, 1995; Jürgens, 2005). Although not assembling a cell plate, animal cytokinesis also depends on membrane fusion events at the midbody (Low *et al*, 2003; Gromley *et al*, 2005; Barr and Grüneberg, 2007; Montagnac *et al*, 2008). In animals and plants, membrane fusion during cytokinesis is mediated by SNARE protein complexes, which include proteins of the syntaxin family (Lauber *et al*, 1997; Jantsch-Plunger and Glotzer, 1999; Xu *et al*, 2002; Low *et al*, 2003; Gromley *et al*, 2005). The *Arabidopsis* KNOLLE syntaxin specifically mediates cytokinetic vesicle fusion (Lauber *et al*, 1997). The restricted expression of KNOLLE from G2/M-phase onward and its accumulation at the cell plate likely mediate its specific function during cytokinesis (Lauber *et al*, 1997; Müller *et al*, 2003; Reichardt *et al*, 2007). How KNOLLE becomes confined to the plane of cell division remains elusive, as do the mechanisms that keep syntaxins in place at the midbody. Strikingly, pharmacological and genetic interference with the biosynthesis of membrane sterols causes cytokinesis defects in human and plant cells (Schrick *et al*, 2000, 2002, 2004;

Fernandez *et al*, 2004; Men *et al*, 2008). Several sterol biosynthesis mutants of *Arabidopsis* including *sterol methyltransferase1* (*smt1*) (Schrick *et al*, 2002, 2004) and *cyclopropylsterol isomerase1-1* (*cpi1-1*) (Men *et al*, 2008) display cytokinesis defects including multinucleate cells, incomplete formation of the cell plate or of the newly formed cross-walls (Schrick *et al*, 2000, 2002, 2004; Men *et al*, 2008). Interestingly, the *cpi1-1* mutant has been found to be defective in the internalization of the endocytic tracer FM4-64 and the *Arabidopsis* PIN2 protein from PMs of dividing and post-cytokinetic root epidermal cells (Men *et al*, 2008). Here, we investigate whether sterol composition and components of the endocytic machinery modulate specificity of KNOLLE syntaxin localization during late cytokinesis.

Results

Altered sterol composition induces KNOLLE accumulation at lateral PMs during late cytokinesis

To address whether altered sterol composition affects KNOLLE protein localization, we immunolocalized KNOLLE in the root meristem of *Arabidopsis* seedlings defective in sterol biosynthesis genes or treated with a sterol biosynthesis inhibitor. We used the *cpi1-1* mutant, which produces cyclopropylsterols as main sterol components (Men *et al*, 2008) and two *smt1* mutants that accumulate cholesterol above wild-type levels (Schrick *et al*, 2002; Willemsen *et al*, 2003). Alternatively, we included the sterol biosynthesis inhibitor fenpropimorph (fen) into the growth medium, at concentrations known to induce strong cyclopropylsterol accumulation (He *et al*, 2003). In contrast to the wild type, which displayed KNOLLE localization in the plane of cell division (Figure 1A and C; Supplementary Figure 1A–I), KNOLLE could be observed at lateral PMs in *cpi1-1* mutant cells, cells of fen-treated roots, $smt1^{orc}$ and $smt1^{cphG213}$ mutant root cells after cell-plate fusion (Figure 1B, D–F). In contrast, we never observed lateral KNOLLE mis-localization during earlier stages of the cell cycle (Supplementary Figure 1J–R), suggesting that KNOLLE localization in the plane of cell division critically depends on correct sterol composition after cell-plate fusion. The cell-plate-localized proteins RAB-A2a fused to yellow fluorescent protein (YFP-RAB-A2a) (Figure 1H) as well as DYNAMIN-RELATED PROTEIN1A (DRP1A)-GFP (also known as ADL1A-GFP; Kang *et al*, 2003) (Figure 1N) did not display the lateral mis-localization observed for KNOLLE in the *cpi1-1* mutant background (Figure 1G–R), suggesting some specificity of this effect to KNOLLE. We focused subsequent analyses on the *cpi1-1* mutant, because it displays the strongest alteration in sterol composition of known sterol biosynthesis mutants (Men *et al*, 2008) and revealed KNOLLE mis-localization at the lateral PM in 43% of late cytokinetic cells.

cpi1-1;knolle double mutant analysis suggests that sterols and KNOLLE act in one pathway

To elucidate the genetic relationship between *KNOLLE* and *CPI1*, we generated *cpi1-1/+;*$knolle^{X37\text{-}2}$*/+* heterozygous plants. These self-pollinated plants produced no seedling progeny (0/951) that deviated from the wild-type, *cpi1-1* or $knolle^{X37\text{-}2}$ phenotypes. An enhancement of the *knolle* phenotype resulting in early embryonic lethality, as earlier reported for the *knolle;keule* double mutant (Waizenegger

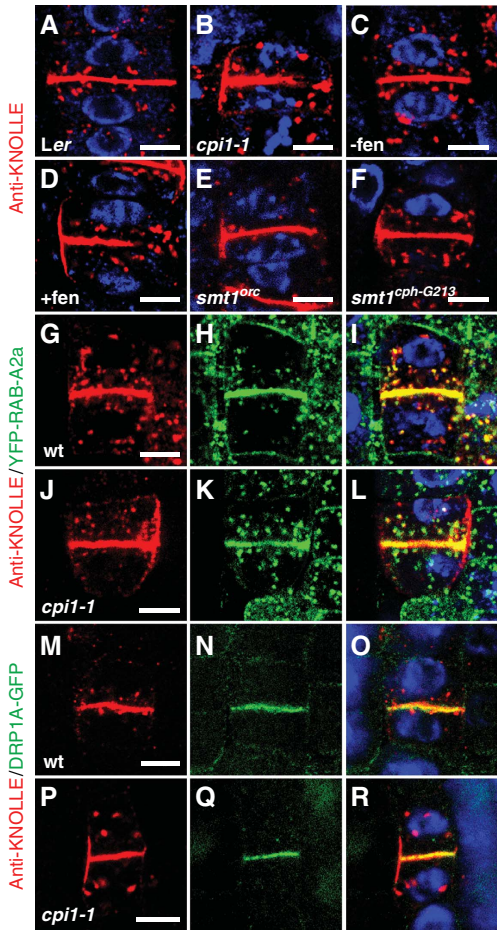

Figure 1 Sterol composition specifies KNOLLE syntaxin localization at the end of cytokinesis. (**A**–**R**) KNOLLE whole-mount immunofluorescence localization (red) in late cytokinetic cells from root tips of 5-day-old *Arabidopsis* seedlings. DAPI staining of DNA (blue). (**A**) Wild-type Landsberg *erecta* (Ler). (**B**) *cpi1-1* mutant. (**C**) Wild-type Columbia-0 (Col-0) without inhibitor treatment (−fen). (**D**) Cell from Col-0 seedling grown on a growth-agar plate including 200 μg/ml fen (+fen). (**E**) $smt1^{orc}$. (**F**) $smt1^{cph\text{-}G213}$. (**G**–**R**) KNOLLE fluorescence co-labelling with fluorescent-protein fusions of other cell-plate proteins (green). (**G**–**I**, **M**–**O**) Wild type (wt). (**J**–**L**, **P**–**R**) *cpi1-1*. (**H**, **K**) YFP-RAB-A2a. (**I**) Merged image of (**G**, **H**) and DAPI. (**L**) Merged image of (**J**, **K**) and DAPI. (**N**, **Q**) DRP1A-GFP. (**O**) Merged image of (**M**, **N**) and DAPI. (**R**) Merged image of (**P**, **Q**) and DAPI. Scale bars are 5 μm. Immunolabelling experiments were performed at least three independent times using a total of 25–30 roots per genotype or treatment.

et al, 2000), was not observed. Instead, molecular genotyping of seedlings displaying the $knolle^{X37\text{-}2}$ developmental phenotype identified 31% of the plants as *cpi1-1;*$knolle^{X37\text{-}2}$ double mutants (13/42) (Figure 2A–C), indicating that *knolle* was epistatic to *cpi1* and suggesting that *KNOLLE* and *CPI1* act in a common pathway.

Co-localization of sterols and KNOLLE at the cell plate and in endomembrane compartments

We subsequently investigated co-localization of KNOLLE and sterols in cytokinetic cells, using filipin III as a 3β-hydroxy-sterol-specific probe in fluorescence co-labelling studies with KNOLLE antibodies and fluorescent-protein markers for the endomembrane system (Grebe *et al*, 2003). KNOLLE and sterols co-localized at the cell plate from the earliest stages

of cell-plate formation until the end of cytokinesis, but co-labelling was also observed at additional endomembrane compartments (Figure 2D–F; Supplementary Figure 1A–I). We quantified co-localization of the geometrical centres of compartments labelled in two different channels, revealing the highest degree of co-localization for sterol and KNOLLE-labelled compartments (Figure 2D–F and P), when compared with all other markers examined (Figure 2G–P; Supplementary Figure 1S–G′). Nevertheless, strong co-localization was also observed between filipin–sterol label and the early endosomal (EE)/*trans*-Golgi network (TGN) markers YFP-RAB-A2a (Figure 2G–I and P) and ADP-RIBOSYLATION FACTOR1 (ARF1)-GFP (Figure 2J–L and P). Filipin–sterol label showed less co-localization with the EE/TGN-marker VHA-a1-GFP (Figure 2P; Supplementary Figure 1S–U), the *trans*-Golgi-marker *N*-ST-YFP (Figure 2P; Supplementary Figure 1Y–A′) and the *medial*-Golgi-marker NAG1-EGFP (Figure 2P; Supplementary Figure 1B′–D′), whereas an endoplasmic reticulum (ER) marker did not display significant co-localization (Figure 2P; Supplementary Figure 1E′–G′; Grebe *et al*, 2003). Analyses of the pre-vacuolar compartment markers RAB-F1-GFP and GFP-RAB-F2b (also known as Ara6-GFP and GFP-Ara7; Ueda *et al*, 2001) confirmed that sterols co-label with these Rab5-type GTPases (Figure 2M–O and P; Supplementary Figure 1V–X), but quantitative analysis revealed a higher degree of co-localization between sterols and KNOLLE as well as other EE/TGN compartment markers (Figure 2P).

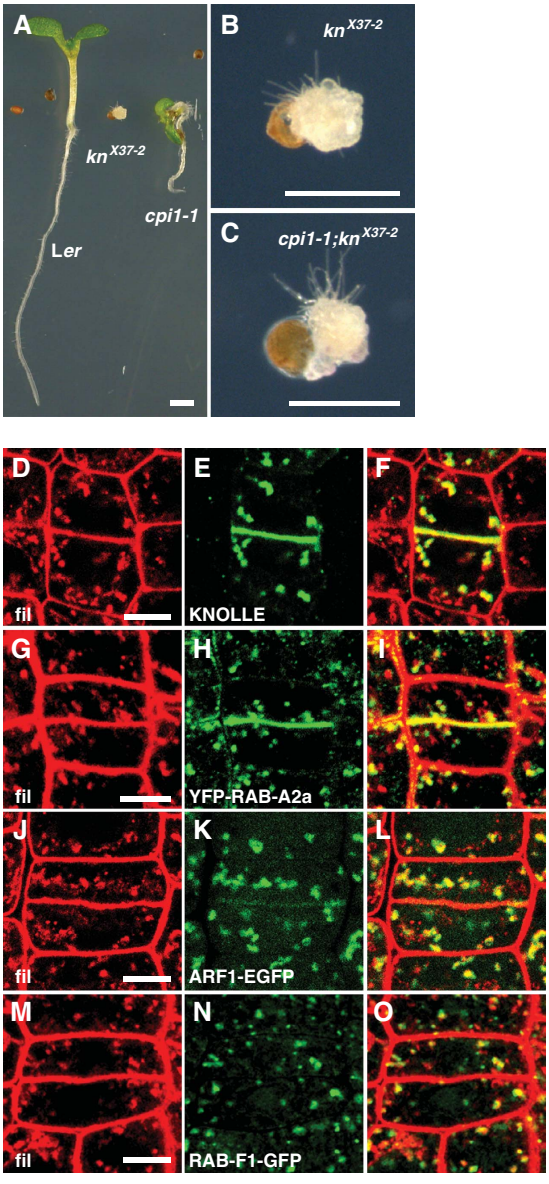

Ultrastructural analysis of filipin–sterol complexes reveals enrichment at the TGN, multivesicular bodies, cell plate and plane of cell division

We next observed filipin–sterol-labelled structures by transmission electron microscopic (TEM) analyses, because filipin–sterol complexes induce specific 20–30 nm membrane deformations on sterol-enriched membranes, which can be visualized in diverse eukaryotic cells (Orci *et al*, 1981; Miller, 1984; Grebe *et al*, 2003). We had earlier described filipin–sterol complexes at the PM of *Arabidopsis* root epidermal cells (Grebe *et al*, 2003). Analyses of cytokinetic root cells revealed clear 20–30 nm deformations at unfused cell-plate membranes (Figure 3A and B) and fully fused cell plates in the plane of cell division (Figure 3C). In comparison, membranes of control cells, which did not contain filipin in the fixative did not display deformations (Figure 3E–G).

Figure 2 Sterols and KNOLLE co-localize and act in a common pathway. (**A**–**C**) Phenotypes of genotyped 5-day-old seedlings from the progeny of a *cpi1-1*/+;*knolle*$^{X37-2}$/+ heterozygote plant (see Supplementary data). (**A**) Wild-type (L*er*), *knolle*$^{X37-2}$ (*kn*$^{X37-2}$) and *cpi1-1*. (**B**) Close up of *kn*$^{X37-2}$ seedling from (**A**). (**C**) *cpi1-1*;*kn*$^{X37-2}$ double mutant. (**D**–**O**) Co-detection of filipin–sterol fluorescence (fil; red) and anti-KNOLLE immunofluorescence labelling or fluorescent-protein fusions to different endomembrane markers (green) in cells at the end of cytokinesis. (**D**, **G**, **J**, **M**) Filipin–sterol fluorescence (fil). (**E**) Anti-KNOLLE (KNOLLE). (**H**) pRAB-A2a:YFP-RAB-A2a (YFP-RAB-A2a). (**K**) pARF1:ARF1-EGFP (ARF1-GFP). (**N**) pRAB-F1:RAB-F1-GFP (RAB-F1-GFP). (**F**, **I**, **L**, **O**) Merged images of the two images to the left, respectively. (**P**) Quantitative co-localization analysis between KNOLLE-immunofluorescence or fluorescent-protein-labelled endomembrane compartments co-labelled with filipin–sterol fluorescence in cytokinetic cells expressed as the percentage (%) of compartments co-localizing with sterols. Data is derived from CLSM images such as in (**D**–**O**) scoring co-localization of the geometrical centres of the two labelled objects within the resolution limit of the microscope objective. Data are mean ± s.d. from 14 cells per marker ($n = 14$). Markers were anti-KNOLLE (KNOLLE), pARF1:ARF1-EGFP (ARF1), pRAB-A2a:YFP-RAB-A2a (RAB-A2a), pVHA-a1:VHA-a1-GFP (VHA-a1), pRAB-F1:RAB-F1-GFP (RAB-F1), p35S:RAB-F2b-GFP (RAB-F2b), p35S:N-ST-YFP (N-ST), p35S:NAG1-EGFP (NAG1), p35S:ER-mGFP5-HDEL (HDEL). Preferential subcellular localization is indicated and colour coded.

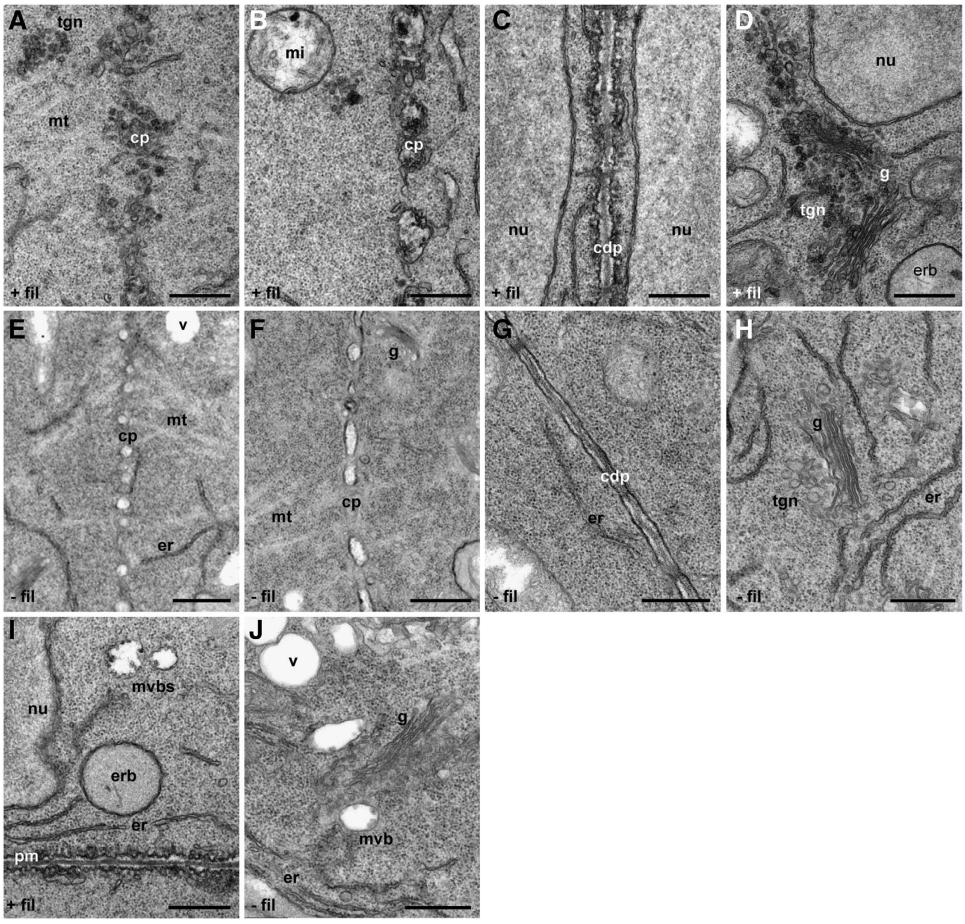

Figure 3 Ultrastructural detection of filipin–sterol complexes at forming and fused cell plates, TGN and MVBs. (**A–J**) TEM images of 80 nm ultrathin sections from cytokinetic epidermal cells of chemically fixed *Arabidopsis* roots embedded in Spurr epoxy-resin (**A–D**, **I**) Filipin-labelled (+fil). (**E–H**, **J**) DMSO solvent without filipin (−fil). (**A–C**) Note, 20–30 nm filipin–sterol complex deformations of *trans*-Golgi network (tgn), unfused cell-plate membranes/vesicles (cp) and fused cell-plate membranes in the plane of cell division (cdp), compared with (**E–G**) smooth membranes in samples not treated with filipin. (**D**) Filipin–sterol complex deformations at tgn compared with (**H**) smooth Golgi (g) membranes in samples not treated with filipin. (**I**) Filipin–sterol complexes at multi-vesicular body (mvb) membranes and plasma membrane (pm). (**H**, **J**) Smooth tgn and mvb membranes in sample not treated with filipin. (**A–J**) Endoplasmic reticulum (er), ER-body (erb), microtubule (mt), nucleus (nu), microtubule (mt), mitochondrion (mi), vacuole (v). Scale bars are 500 nm.

Strikingly, the TGNs of filipin-labelled samples revealed strong 20–30 nm deformations starting from the *trans*-most Golgi cisternae (Figure 3A and D), compared with control cells that displayed the expected smooth morphology of TGN vesicles and unaffected *trans*-most Golgi cisternae (Figure 3H). In contrast, filipin treatment did neither affect the membranes of the *cis*- and *medial*-Golgi cisternae (Figure 3D and H), nor ER and nuclear envelope membranes (Figure 3C, D and I), whereas multivesicular bodies (MVBs) displayed clear deformations of their outer membranes (Figure 3I), when compared with the smooth membrane of MVBs in non-treated samples (Figure 3J). These observations corroborated the results obtained from filipin–sterol fluorescence microscopy, showing a stronger accumulation of filipin–sterol complexes at the TGN, *trans*-Golgi and MVBs compared with the *medial*- and *cis*-Golgi cisternae as well as the ER. These results showed remarkable similarities to the heterogenous distribution of sterols over the cisternae of the Golgi apparatus (Orci *et al*, 1981) and the enrichment of sterols in the endocytic pathway in mammalian cells (Möbius *et al*, 2003). Hence, our findings suggest a graded accumulation of sterols throughout the plant endomembrane system, revealing a high degree of co-localization of sterols and KNOLLE at the TGN/EE, the cell plate and in the plane of cell division.

KNOLLE is not enriched in detergent-resistant membrane fractions

The TGN in yeast cells has been indicated to have the capacity to sort sterols and sphingolipids together with specific protein cargo on its way to the PM (Klemm *et al*, 2009). Owing to the co-localization of sterols and KNOLLE at TGN and cell-plate membranes, we investigated a potential enrichment of KNOLLE in detergent-resistant membranes (DRMs) thought to contain sterol and sphingolipid-enriched microdomains, sometimes referred to as 'lipid rafts' or 'membrane rafts' (Simons and Ikonen, 1997; Mongrand *et al*, 2004; Borner *et al*, 2005; Pike, 2006; Zappel and Panstruga, 2008; Boutté and Grebe, 2009). Membrane rafts contribute to lateral compartmentalization of membranes (Simons and Ikonen, 1997; Pike, 2006), but their *in vivo* existence and *in vivo* function in plant membranes remain poorly addressed (Zappel and Panstruga, 2008; Boutté and Grebe, 2009). We isolated the total membrane (TM) fraction

from an *Arabidopsis* cell suspension culture, subjected it to DRM extraction, using different ratios of the detergent Triton-X-100 versus TM protein, and isolated the DRM fraction by sucrose-density-gradient centrifugation (Borner *et al*, 2005). Subsequently, we analysed the protein content by probing western blots with antibodies directed against DRM-enriched PM-H^+-ATPase and the DRM-depleted ER chaperone BiP (Mongrand *et al*, 2004; Borner *et al*, 2005). In addition, we generated an antiserum that specifically detected the integral membrane protein SMT1, which co-localized with ER markers in immunofluorescence co-labelling studies (Supplementary Figure 2). In contrast to PM-H^+-ATPase, but similar to BiP and SMT1, KNOLLE was depleted from DRMs at the moderate detergent to protein ratio of 4, and slightly less depleted, when compared with SMT1 and BIP at the ratio of 8, but not enriched, when compared with the TM or mock-treated fraction (Figure 4; Supplementary Figure 3). Hence, interference with KNOLLE localization in 'lipid rafts' is unlikely to account for its lateral mis-localization at the PM observed on altered sterol composition.

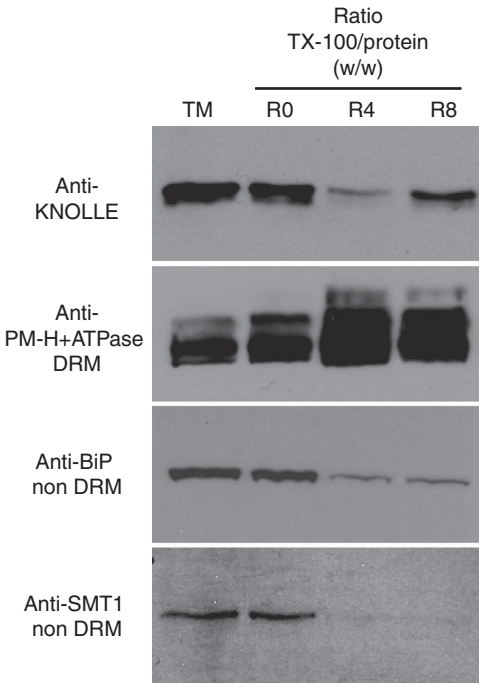

Figure 4 KNOLLE is not enriched in DRM fractions. Western-blot analysis of proteins in DRM fractions extracted from an *Arabidopsis* cell suspension culture. Equal amounts of membrane protein (4 μg) were loaded from total membrane (TM) fraction, the floating fraction mock extracted at Triton-X-100 (TX-100) detergent/protein ratio 0 (R0), DRM fractions after extraction at ratio 4 (R4) and ratio 8 (R8). Antibodies were directed against KNOLLE, the DRM-enriched marker protein(s) PM-H^+ATPase (DRM), the DRM-depleted (non-DRM) proteins BiP and SMT1. Similar results were obtained in three independent experiments.

The cpi1-1 mutation does not obviously enhance KNOLLE lateral diffusion at or secretory targeting to the PM

To address the possibility that sterol composition may affect KNOLLE mobility from the plane of cell division to lateral membranes, we analysed lateral mobility of KNOLLE by fluorescence-recovery-after-photo-bleaching (FRAP) experiments. To this end, we used seedlings that expressed a functional GFP-KNOLLE protein, which rescues the *knolle* mutant phenotype (Reichardt *et al*, 2007). On photo-bleaching of GFP-KNOLLE within a 2 μm membrane region in the plane of cell division, FRAP occurred in this area (Figure 5A–C). Recovery was slightly faster than in roots incubated with energy inhibitors (sodium azide and 2-deoxy-D-glucose) (Figure 5A–C), which abolishes energy-dependent traffic and allows assessing the contribution of diffusion to lateral mobility (Men *et al*, 2008). Similarly, when the membranes in the plane of cell division were bleached completely in roots incubated with the protein biosynthesis inhibitor CHX or energy inhibitors and CHX, recovery was slower in energy inhibitor-treated cells (Supplementary Figure 4A–C). We infer that both membrane trafficking and lateral diffusion contribute to fluorescence recovery of GFP-KNOLLE in the plane of cell division, because energy-inhibitor-treated roots displayed significantly reduced but still substantial recovery (Figure 5C; Supplementary Figure 4C).

In contrast to native KNOLLE, GFP-KNOLLE is additionally found at the PM just after cytokinesis (Figure 5A) (Reichardt *et al*, 2007). We exploited this property to investigate potential mobility of GFP-KNOLLE from the plane of cell division to lateral membranes. We bleached GFP-KNOLLE fluorescence from newly formed daughter cells at the end of cytokinesis, except for the fluorescence in the plane of cell division (Figure 5D, E and G). Subsequently, we monitored

Figure 5 KNOLLE lateral diffusion from the cell-division plane is not altered in the *cpi1-1* mutant. (**A–N**) FRAP analyses combined with (**D–K**) FLIP analyses of GFP-KNOLLE fluorescence. (**A**, **B**, **D**, **E**, **G**, **I**, **J**, **L**, **M**) Pre-bleach (pre), post-bleach (post) and subsequent post-bleach images acquired at time points in minutes. Boxes indicate bleach ROIs. (**A–C**) FRAP analyses after bleaching of a 2 μm ROI in the plane of cell division in (**A**) wild type (wt) or in (**B**) wild type after 45 min pre-incubation with energy inhibitors (-e), 0.02% sodium azide, 50 mM 2-deoxy-D-glucose (wt -e). (**C**) Quantitative analyses of experiments such as in (**A**, **B**) showing normalized values of pre- and post-bleach fluorescence intensities at recovery time points in 30 s post-bleach image acquisition intervals. Data are mean ± s.d. from 14 cells ($n = 14$). (**D**, **E**) Bleaching of GFP-KNOLLE at the end of cytokinesis, except for fluorescence in the plane of cell division, in phenotypically wild-type (wt, +/+ and *cpi1-1*/+) offspring from a *cpi1-1*/+;*GFP-KNOLLE* plant. (**D**) 45 min, 50 μM CHX (wt CHX). (**E**) 45 min, 50 μM CHX,-e (wt CHX -e). (**F**) Quantitative analyses of experiments such as in (**D**, **E**) for FLIP at membranes in the cell-division plane (CP) and FRAP at the outer plasma membrane (PM) under CHX or CHX,-e application, respectively. Data are mean ± s.d. from 10 cells ($n = 10$). (**G**) as E, but in *cpi1-1*;*GFP-KNOLLE* background (*cpi1-1* CHX -e). (**H**) Quantitative comparison of experiments such as in (**E**, **G**) for FLIP at the CP and FRAP at the PM. Data are mean ± s.d. from 10 cells ($n = 10$). (**I**, **J**) Bleaching of GFP-KNOLLE at the plane of cell division in (**I**) wild type and (**J**) *cpi1-1* mutant both pre-treated 45 min, 50 μM CHX,-e (wt CHX -e). (**K**) Quantitative comparison of experiments such as in (**I**, **J**) for FLIP at the PM and FRAP at the CP. Data are mean ± s.d. from seven cells ($n = 7$). (**L**, **M**) GFP-KNOLLE FRAP in fully bleached (**L**) *cpi1-1*/+ or +/+ and (M) *cpi1-1* cells. (**N**) Quantitative comparison of FRAP experiments such as in (**L**, **M**). Data are mean ± s.d. from 10 cells ($n = 10$). (**O–Q**) KNOLLE immunofluorescence localization (red) in late cytokinetic cells of L*er* seedling roots with or without inhibitor treatment. DAPI DNA staining (blue). (**O**) L*er*. (**P**) L*er*, 30 min, 50 μM CHX. (**Q**) L*er*, 30 min, 50 μM CHX -e. All scale bars are 5 μm.

FRAP at the PM and fluorescence-loss-in-photo-bleaching (FLIP) in the plane of cell division (Figure 5D–H). These experiments were performed on roots pre-treated with CHX (Figure 5D and F) to monitor lateral relocation of GFP-KNOLLE in the absence of protein biosynthesis. We also examined the effects of pre-treatment with CHX and energy inhibitors to assess GFP-KNOLLE lateral diffusion (Figure 5E and F). On both treatments, FRAP started from the sites in which the cell-plate membrane had contacted the PM and fluorescence progressively spread over the lateral membranes, until it had recovered over the total PM (Figure 5D and E). FRAP at the PM and FLIP in the plane of cell division closely complemented each other, both in cells treated with CHX or CHX and energy inhibitors (Figure 5F), strongly

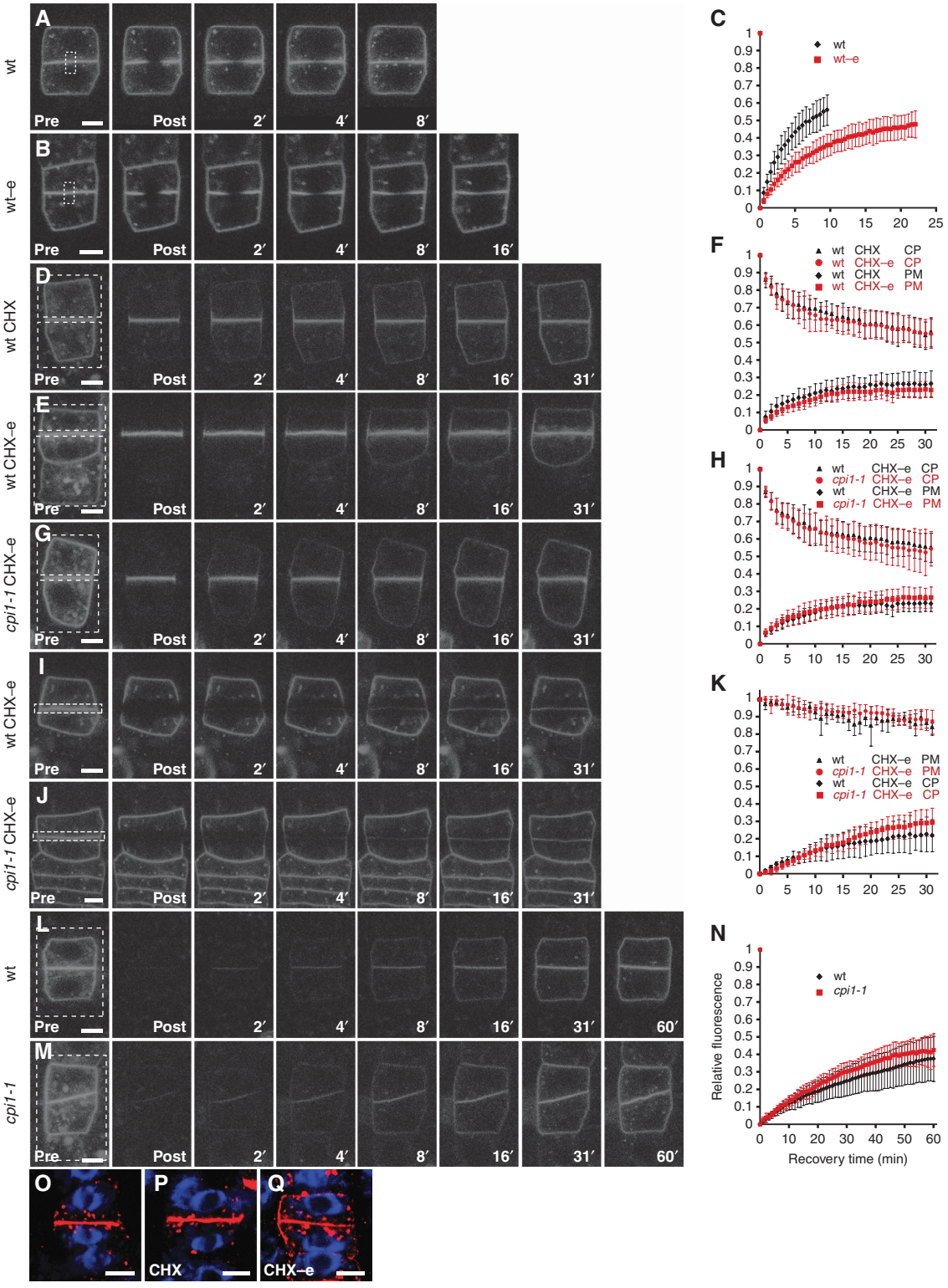

suggesting that GFP-KNOLLE relocated from the plane of cell division by lateral diffusion. We did not observe a difference between FLIP or FRAP of GFP-KNOLLE in wild type and in *cpi1-1* mutant cells treated with CHX and energy inhibitors (Figure 5E, G and H). Similarly, FLIP and FRAP kinetics monitoring lateral diffusion did not obviously differ between wild-type and *cpi1-1* mutant cells in which fluorescence had been bleached at the membranes in the plane of cell division (Figure 5I, J and K). Therefore, altered sterol composition is unlikely to directly affect the rate of GFP-KNOLLE lateral diffusion when membrane trafficking is blocked. Moreover, we did not observe a significant difference between the FRAP kinetics of wild-type and *cpi1-1* mutant cells in which GFP-KNOLLE fluorescence had been bleached completely (Figure 5L–N), indicating that secretory trafficking of GFP-KNOLLE was not substantially affected in the mutant. Taken together, our findings show that GFP-KNOLLE can move from the plane of cell division to the PM and vice versa by lateral diffusion, which does not *per se* appear to be affected in the *cpi1-1* mutant.

Enhanced lateral diffusion of GFP-KNOLLE may potentially be difficult to detect in the *cpi1-1* mutant, because functional GFP-KNOLLE, unlike the native endogenous KNOLLE protein, already displays some PM localization in the wild type. We, therefore, compared lateral diffusion of GFP-KNOLLE and additional molecules, the small styryl dye FM4-64, the small integral PM protein EGFP-LTI6a and the larger functional PIN2-EGFP protein into a 4 μm region at the lateral membrane of late cytokinetic cells. By taking this approach, we covered a large range of lateral diffusion rates displayed by these molecules (Supplementary Figure 4D). However, none of them displayed obviously faster lateral diffusion in the *cpi1-1* mutant, when compared with the wild type (Supplementary Figure 4E–P), suggesting that lateral diffusion of diverse molecules is not *per se* enhanced in the *cpi1-1* mutant background.

To explore whether native, endogenous KNOLLE can diffuse laterally, we examined its localization in roots treated with CHX or CHX and energy inhibitors. In contrast to cells of untreated and CHX-treated roots (Figure 5O and P), we observed KNOLLE lateral mis-localization in cells of CHX plus energy-inhibitor-treated roots (Figure 5Q). KNOLLE lateral localization appeared to be particularly sensitive to energy inhibition, when compared with PIN2 and DRP1A-GFP, which did not laterally relocate within the same time (Supplementary Figure 5A–L and M–U), whereas YFP-RAB-A2a fluorescence in the cell division plane rapidly decreased after application of energy inhibitors (Supplementary Figure 5V-D′), consistent with the view that this small Rab GTPase associates with the membrane in its GTP-bound form. Our results suggest that native KNOLLE can diffuse toward lateral membranes, which normally appears to be compensated for by an energy-dependent mechanism such as endocytic trafficking.

KNOLLE endocytosis at the end of cytokinesis is altered in the cpi1-1 mutant

The endocytic tracer FM4-64 rapidly co-labels with GFP-KNOLLE in the developing cell plate (Reichardt *et al*, 2007). Shortly after application, FM4-64 also co-localized with GFP-KNOLLE in small, punctuate structures in CHX-pre-treated cells whose cell plates had just fused with the PM (Figure 6A–C). These endosomes displayed reactivity to the endocytic recycling inhibitor brefeldin A (BFA; Geldner *et al*, 2001; Geldner *et al*, 2003; Grebe *et al*, 2003) (Figure 6D–F) that, 60 min after its application, induced co-accumulation of GFP-KNOLLE and FM4-64 in larger 'BFA compartments' (Figure 6G–I). We subsequently analysed the behaviour of native KNOLLE in CHX and BFA-treated cells. After 60 min of treatment, KNOLLE immunofluorescence was reduced at the cell division plane, but accumulated in BFA compartments in both the wild type and the *cpi1-1* mutant during late cytokinesis (Figure 6J–M). This was quantitatively reflected in a strongly decreased ratio of relative KNOLLE fluorescence at the cell division plane to label found in intracellular compartments after 60 min of BFA treatment (Figure 6N). In comparison with wild type (Figure 6K), more KNOLLE label was retained in the plane of cell division in the *cpi1-1* mutant 60 min after BFA application (Figure 6M), which was reflected in a higher fluorescence intensity ratio in the *cpi1-1* mutant when compared with wild type (Figure 6N). Together with the FM4-64 and PIN2 internalization defects observed in the *cpi1-1* mutant (Men *et al*, 2008), these findings suggest that correct membrane sterol composition is required for KNOLLE endocytosis at the end of cytokinesis.

Sterol localization to KNOLLE-positive, TGN and MVB compartments is altered in the cpi1-1 mutant

We next examined the association of sterols with compartments of the endocytic pathway, including KNOLLE-positive structures, in the *cpi1-1* mutant. Quantitative co-localization analyses (Supplementary Figure 6Q′) revealed a lower percentage of KNOLLE-positive endomembrane structures co-localizing with filipin–sterol fluorescence in *cpi1-1* (Supplementary Figure 1P–R) when compared with wild type (Supplementary Figures 1G–I and 6Q′). Similarly, in the *cpi1-1* mutant, reduced co-localization with filipin–sterol fluorescence was observed for ARF1-GFP (Supplementary Figure 6A–C, V–X and Q′) and YFP-RAB-A2a-positive TGN/EE compartments (Supplementary Figure 6D–F, Y-A′ and Q′) as well as RAB-F1-GFP (Supplementary Figure 6J–L, E′–G′ and Q′) and GFP-RAB-F2b positive later endosomal compartments (Supplementary Figure 6M–O, H′–J′ and Q′). However, the total number of filipin–sterol-labelled structures in *cpi1-1* mutant cells was not reduced when compared with the wild type (data not shown), showing that this result was not because of a lower-labelling efficiency in the mutant background. Consistent with this view, the percentage of NAG1-EGFP-labelled Golgi stacks co-labelling with filipin–sterol fluorescence was increased in the *cpi1-1* mutant when compared with the wild type (Supplementary Figure 6P–R, K′–M′ and Q′), corroborating biochemical studies reporting accumulation of sterols in the Golgi-containing membrane fraction on pharmacological interference with cyclopropylsterol isomerization (Laloi *et al*, 2007). Hence, the *cpi1-1* mutation reduced sterol accumulation within the population of KNOLLE-positive, early endocytic/TGN and later endocytic/MVB compartments, further suggesting a defect in the endocytic pathway of this mutant.

KNOLLE accumulation at lateral PMs in endocytosis-defective arf1^{T31N} expressing plants

To address whether altered endocytosis causes lateral mis-localization of KNOLLE, we examined its subcellular

distribution after interference with ARF1 function by a dominant-negative approach, earlier reported to affect internalization of the endocytic tracer FM4-64 (Xu and Scheres, 2005). To this end, we analysed KNOLLE localization in plants expressing a heat-shock-induced dominant-negative arf1^{T31N}-CFP mutant version. In contrast to roots expressing wild-type ARF1-GFP under control of its own promoter or a heat-shock promoter (Figure 7A–H and T), arf1^{T31N}-CFP expression caused lateral mis-localization of KNOLLE during late cytokinesis (Figure 7I–L and T). As, similar to ARF1, we had observed sterol co-localization with the EE/recycling endosomal Rab11-like RAB-A2a GTPase, as well as the RAB-F1 and RAB-F2b GTPases located at later endosomal compartments, we wondered as to whether interference with RAB-A2a or RAB-F function would affect KNOLLE and sterol localization. We, therefore, analysed the *vps9a-2* mutant, defective in the main RAB-F guanine-nucleotide exchange factor (Goh *et al*, 2007) as well as plants expressing a rab-A2a^{N125I} dominant-negative mutant version for KNOLLE and sterol accumulation. In contrast to arf1^{T31N}-CFP roots, KNOLLE accumulation at the PM was neither observed in the roots expressing rab-A2a^{N125I} (Supplementary Figure 7A–F) nor in *vps9a-2* mutant roots (Supplementary Figure 7G–L). Strikingly, however, both rab-A2a^{N125I} expressing and *vps9a-2* mutant plants co-accumulated sterols and KNOLLE in endomembrane compartments (Supplementary Figure 7D–F and J–L), suggesting that these mutations do not primarily cause a defect in KNOLLE internalization from the PM, but rather interfere with KNOLLE and sterol trafficking at endosomal compartments. Taken together, interference with ARF1 caused defects in internalization of an endocytic tracer from the PM (Xu and Scheres, 2005) and lateral mis-localization of KNOLLE during late cytokinesis, further suggesting that defective internalization may result in a failure to limit KNOLLE lateral diffusion.

KNOLLE accumulates at the PM after tyrphostin A23 treatment and in endocytosis-defective drp1A mutants

To investigate whether clathrin-dependent endocytosis mediates KNOLLE internalization and restricts KNOLLE localization to the plane of cell division, we treated plants with tyrphostin A23 (TyrA23), an inhibitor of recruitment of endocytic cargo into the clathrin-mediated pathway (Ortiz-Zapater *et al*, 2006; Dhonukshe *et al*, 2007). When compared with untreated cells (Figure 7M and T; Supplementary Figure 7M–O), short-term TyrA23 treatment induced KNOLLE mis-localization at lateral membranes in late cytokinesis (Figure 7N and T; Supplementary Figure 7P–R), which was not observed in cells treated with the inactive analogue TyrA51 (Figure 7O and T; Supplementary Figure 7S–U). Moreover, this TyrA23 effect was reversible after washout of the drug (Figure 7P). Consistent with the view that KNOLLE internalization is mediated by clathrin-dependent endocytosis, KNOLLE displayed substantial co-localization with

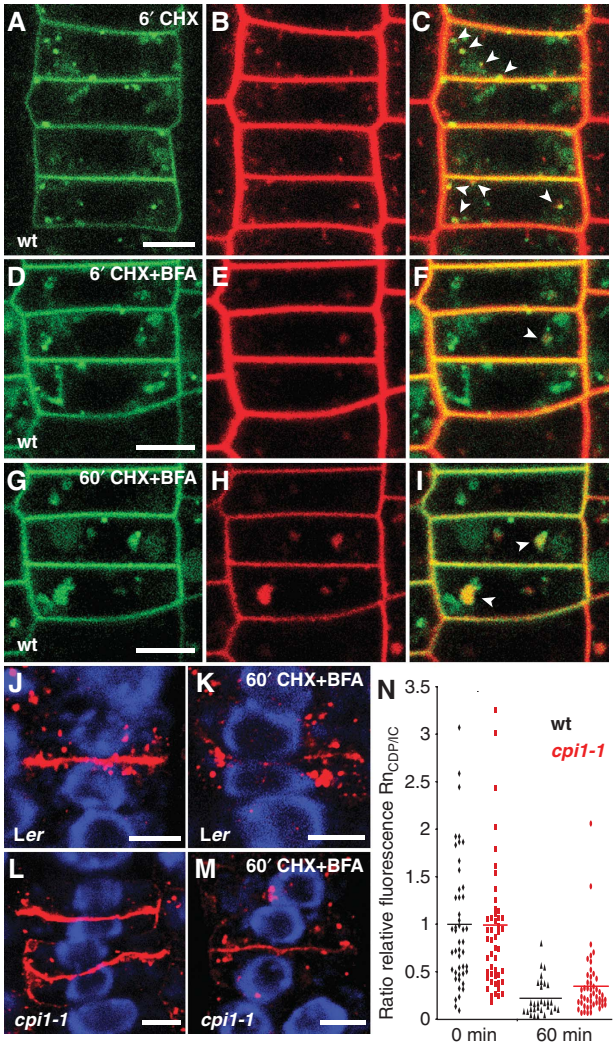

Figure 6 At the end of cytokinesis KNOLLE internalizes through early endosomes, but is more retained at the plane of cell division in *cpi1-1*. (**A**, **D**, **G**) GFP-KNOLLE fluorescence and (**B**, **E**, **H**) FM4-64 fluorescence in wild type overlaid in (**C**, **F**, **I**). (**A**–**C**) Cells pre-treated 45 min with 50 μM CHX, pulsed with 25 μM FM4-64 for 5 min and incubated were examined for FM4-64 internalization (**D**–**F**) after 6 min and (**G**–**I**) 60 min of incubation with 50 μM CHX, 50 μM BFA. Note co-localization in endosomes between GFP-KNOLLE and FM4-64 (arrowheads in **C**, **F**, **I**). (**J**–**M**) anti-KNOLLE immunolocalization (red) in late cytokinetic cells with DAPI staining for DNA (blue). (**J**) KNOLLE after 45 min of pre-treatment with 50 μM CHX before BFA application (0 min) (**K**) becomes internalized into BFA compartments and disappears from the cell plate after prolonged incubation for 60 min (60′) with 50 μM CHX, 10 μM BFA. (**L**) *cpi1-1* mutant cells after 45 min of pre-treatment with 50 μM CHX and (**M**) prolonged incubation for 60 min (60′) with 50 μM CHX, 10 μM BFA. Note, KNOLLE in plane of cell division in (**M**) compared with (K). (**N**) Quantification of KNOLLE immunofluorescence intensity at the cell-division plane (CDP) versus internal compartments (IC) from experiments in (**J**–**M**). The normalized fluorescence intensity ratio Rn$_{CDP/IC}$ (normalized to time point 0) is given per cell. This was obtained by calculating $R_{CDP/IC}$ = [mean amplitude relative pixel intensity of KNOLLE at CDP: length CDP (μm)]: [mean amplitude relative pixel intensity of KNOLLE label/area IC (μm^2)] per cell and normalizing $R_{CDP/IC}$ by dividing it through the average Rav$_{CDP/IC}$ of the analysed cell population at 0 min (start intensity ratio) for wild type and *cpi1-1*, respectively. Exact *P*-values obtained from non-parametric, two-tailed Mann–Whitney *U*-test were wild type at 0 min ($n = 47$) versus wild type at 60 min ($n = 30$), $P < 2e\text{-}06$; *cpi1-1* at 0 min ($n = 50$) versus *cpi1-1* at 60 min ($n = 49$) $P < 2e\text{-}06$, and wild type at 60 min ($n = 30$) versus *cpi1-1* at 60 min ($n = 49$) $P = 0.0277$ with a significance threshold at $P < 0.05$; *n* indicates the numbers of epidermal cells at the end of cytokinesis analysed and obtained from 18 to 24 roots per genotype or treatment. Scale bars are 5 μm.

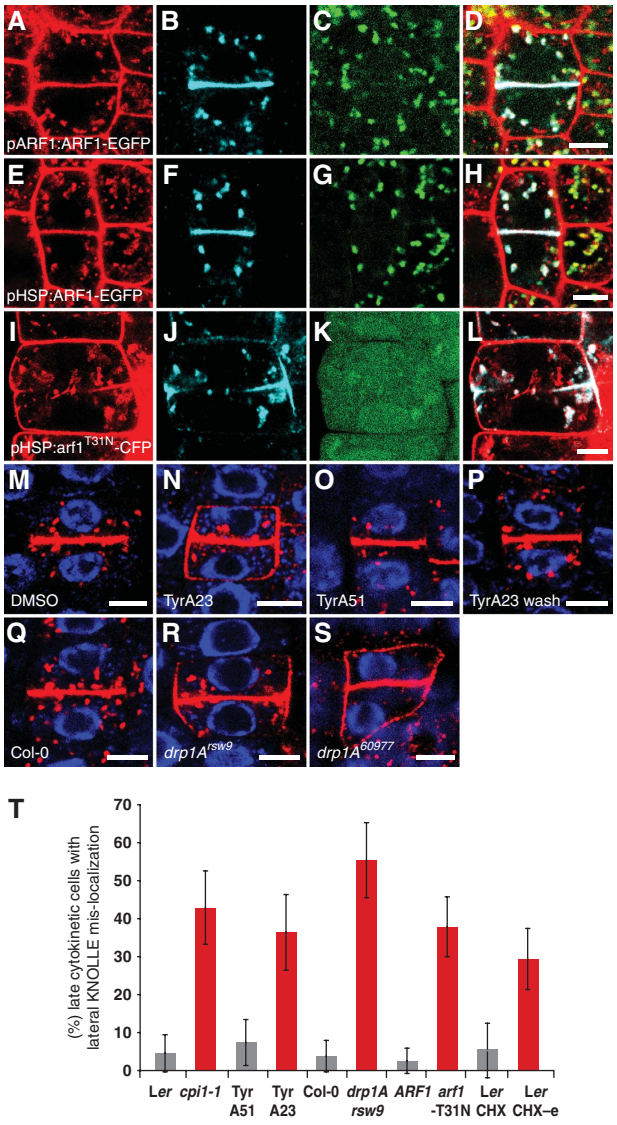

Figure 7 ARF1, clathrin and dynamin-dependent endocytosis restricts KNOLLE to the cell division plane. (**A–S**) KNOLLE immunofluorescence labelling in late cytokinetic cells. (**A–L**) KNOLLE immunofluorescence (cyan) co-labelling with filipin–sterol fluorescence (red) and fluorescent fusion proteins (green). (**A–L**) Heat-shock-treated plants expressing the following ARF1-fluorescent-protein fusions (**A–D**) pARF1:ARF1-GFP (green), (**E–H**) pHSP:ARF1-GFP (green), (**I–L**) pHSP:arf1^{T31N}-CFP (green). (**A**, **E**, **I**) filipin–sterol (**B**, **F**, **J**) anti-KNOLLE. (**D**, **H**, **L**) Merged image of (**A–C**), (**E–G**) and (**I**, **J**), respectively. (**M–S**) anti-KNOLLE immunofluorescence (red) co-labelling with DAPI staining of DNA (blue) of wild-type L*er* treated with (**M**) 1 h, DMSO at 0.2%, (**N**) 1 h, 50 μM Tyrphostin A23 (TyrA23), (**O**) 1 h, 50 μM Tyrphostin A51 (TyrA51), (**P**) 1 h, 50 μM TyrA23 followed by 1 h wash out (wash). (**Q**) Wild-type Col-0, (**R**) *drp1A*^{rsw9}, (**S**) *drp1A*^{SALK_060977} (*drp1A*^{60977}). (**T**) Quantification of the percentage of cells in late cytokinesis displaying lateral KNOLLE mis-localization in roots of indicated genotypes or treatments. Data are mean ± s.d. from 12 to 18 independent roots ($n = 12–18$) with 84–145 cells analysed per genotype or treatment. Scale bars are 5 μm.

CLATHRIN-LIGHT-CHAIN (CLC)-GFP during late cytokinesis (Supplementary Figure 7V–X).

We also addressed whether the dynamin-like protein DRP1A is required for KNOLLE localization, because *drp1a* mutants are defective in endocytosis and cytokinesis

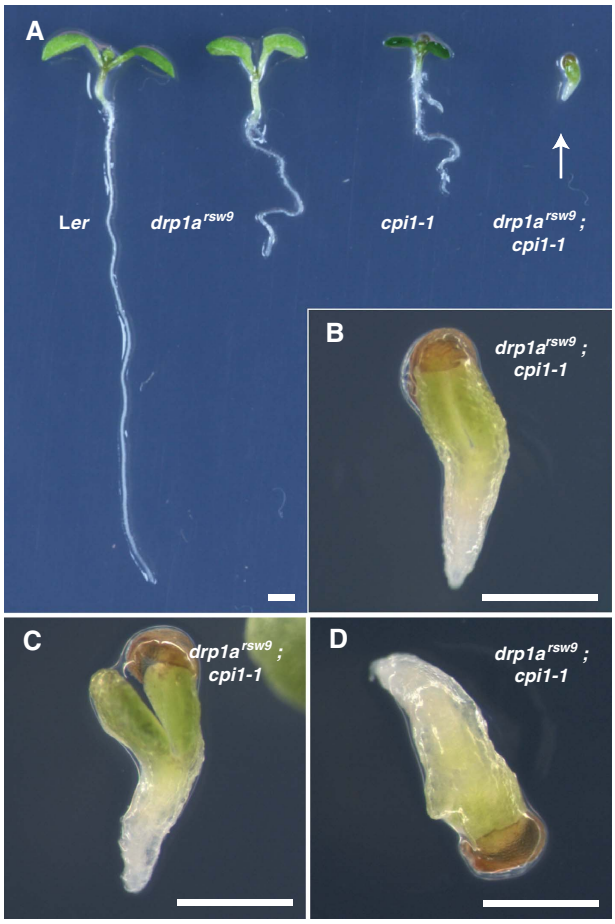

Figure 8 Synergistic genetic interaction between *DRP1A* and *CPI1*. (**A**) Five-day-old seedlings of wild-type Landsberg *erecta* (L*er*), *drp1a*^{rsw9}, *cpi1-1* and a genotyped *drp1a*^{rsw9};*cpi1-1* double mutant. (**B–D**) Five-day-old *drp1a*^{rsw9};*cpi1-1* double mutant seedlings identified by PCR-based genotyping with molecular markers (see Material and methods). (**B**) Higher magnification stereomicroscopy image of seedling in (**A**). Scale bars are 1 mm.

(Collings *et al*, 2008). When compared with the wild type (Figure 7Q and T), KNOLLE displayed profound lateral mis-localization in *drp1a* mutants (Figure 7R, S and T), strongly suggesting that clathrin-dependent endocytosis mediated by DRP1A laterally restricts KNOLLE localization during late cytokinesis.

cpi1-1;drp1a double mutant analysis suggests synergistic action of sterols and DRP1A

The mis-localization of KNOLLE observed in both *drp1a* and *cpi1-1* mutant cells during late cytokinesis prompted us to address the genetic relationship between *DRP1A* and *CPI1*. Analyses of the progeny from a self-pollinated *drp1a*^{rsw9}/*drp1a*^{rsw9};*cpi1-1*/+ plant revealed that 22.6% of seedlings (31/137) displayed a synthetic seedling-lethal phenotype when compared with wild-type, *drp1a*^{rsw9} and *cpi1-1* seedlings (Figure 8A). Such a segregation ratio close to 25% would be expected for a *drp1a*^{rsw9};*cpi1-1* double mutant. Consistent with this notion, no phenotypically *cpi1-1*-looking seedlings were observed in the progeny of *drp1a*^{rsw9}/*drp1a*^{rsw9};*cpi1-1*/+ (0/137). Instead, seedlings that displayed the seedling-lethal phenotype, which showed little variability

(Figure 8B–D), and were subjected to molecular genotyping (see Materials and methods), proved to be *drp1a*^{rsw9};*cpi1-1* homozygous (21/21). This synergistic genetic interaction between *DRP1A* and *CPI1* suggests that their action converges before or at the level of common targets such as endocytosis-dependent KNOLLE localization during late cytokinesis.

Discussion

This study shows that syntaxin localization in the plane of cell division can be focussed through sterol-dependent, clathrin and dynamin-mediated endocytosis at the end of cytokinesis. On interference with endocytosis by treatment with energy inhibitors, KNOLLE diffused from the plane of cell division to lateral membranes, highly similar to the mislocalization observed in endocytosis-defective mutants. Interestingly, establishment of PIN-type auxin efflux carrier polarity also relies on correct sterol composition during asymmetric endocytic removal of PIN2 from the basal membrane directly after cell division (Men *et al*, 2008). Moreover, internalization of PIN1 from lateral and apical membranes mediates basal polarity establishment in elongating cells (Dhonukshe *et al*, 2008) and pharmacological as well as dominant-negative interference with clathrin-dependent endocytosis have been shown to block PIN protein internalization (Dhonukshe *et al*, 2007). Together with this study, these findings highlight the importance of clathrin-mediated internalization during polarity establishment of various cargo molecules in plants. Strikingly, however, KNOLLE eventually becomes internalized from both membranes in the former plane of cell division, whereas PIN2 is retained at one membrane. These findings suggest a specification at the level of PIN protein targeting or recycling to retain them at only one membrane after cytokinesis. Another difference can be observed at the level of lateral diffusion, which is significantly faster for GFP-KNOLLE than for PIN2-EGFP and, consistent with these findings, native KNOLLE displays fast lateral relocation in energy-inhibitor-treated late cytokinetic cell, when compared with native PIN2. Apparently, endocytosis has a larger impact on restricting KNOLLE diffusion from the lateral membrane, when compared with the slower diffusing PIN2 protein. Hence, our findings suggest that, at the end of cytokinesis, endocytosis contributes to keep lateral diffusion of a major mediator of cytokinetic vesicle fusion in check.

Considering that cell-plate fusion rarely occurs synchronized along the complete circumference of the plate (Cutler and Ehrhardt, 2002; Kang *et al*, 2003; Van Damme *et al*, 2006), it is conceivable that local KNOLLE abundance has a critical function during cell-plate fusion. Lateral diffusion may create a lack of KNOLLE at sites that have not undergone fusion, yet. This may cause reduced membrane fusion or cell-wall establishment reflected in the formation of incomplete cell walls that can be observed in mutants defective in KNOLLE-interacting SNAREs, in sterol biosynthesis and *drp1a* mutants (Lauber *et al*, 1997; Schrick *et al*, 2000, 2002, 2004; Collings *et al*, 2008; Men *et al*, 2008). Similarly, reduced expression of *TPLATE* causes cytokinesis defects (Van Damme *et al*, 2006). The TPLATE protein shows similarity to vesicle coat proteins and its localization at the cell plate, as well as a small PM area just adjacent to the site of plate fusion, implicates TPLATE in cell-plate insertion (Van Damme *et al*, 2006). A requirement for KNOLLE at this step is suggested by its accumulation at the edge of the plate during late cytokinesis (Lauber *et al*, 1997) and its lateral mislocalization at sites of cell-plate fusion in the *cpi1-1* and *drp1a* mutants. Together with the endocytosis defects reported for these mutants (Collings *et al*, 2008; Men *et al*, 2008), our analyses of KNOLLE localization suggest that DRP1A and sterols modulate KNOLLE endocytosis in a similar manner, an interpretation that is further supported by the synergistic genetic interaction observed between *DRP1A* and *CPI1*. Finally, pharmacological interference with cyclopropylsterol isomerization increased the residence time of DRP1A-GFP foci at the cell cortex (Konopka and Bednarek, 2008; Konopka *et al*, 2008) and TyrA23 treatment reduced the dynamics of such foci in which CLC and DRP1A co-localized at the cell cortex (Konopka and Bednarek, 2008; Konopka *et al*, 2008). It is, thus, conceivable that altered sterol composition interferes with vesicle budding at the level of clathrin-dependent endocytosis required to restrict KNOLLE to the plane of cell division. Two not necessarily mutually exclusive scenarios can be envisaged as to how DRP1A and clathrin-mediated endocytosis could restrict KNOLLE localization to the plane of cell division. As both KNOLLE and DRP1A accumulate at the leading edge of the cell plate, DRP1A may already be involved in recycling of KNOLLE at this stage. However, weaker DRP1A accumulation is also observed at the (lateral) PM (cf. Figure 1N), and this subpopulation of DRP1A foci may additionally contribute to restrict lateral diffusion of KNOLLE.

Notably, interference with sterol composition affects clathrin- and dynamin-dependent endocytosis in fungal and animal cells (Pichler and Riezman, 2004), but a mechanism for restricting syntaxin localization to the plane of cell division has not been reported for these systems. Interestingly, the centriolin protein is required for syntaxin2 localization at the midbody in human cells (Gromley *et al*, 2005), possibly mediating anchorage of syntaxin2-positive vesicles after delivery (Gromley *et al*, 2005). The recycling endosomal Rab11 and ARF6 GTPases contribute to vesicle recycling at the midbody of mammalian cells (Montagnac *et al*, 2008), but their action on SNARE components has not been addressed. In comparison, our results suggest that sterols, clathrin, DRP1A and ARF1-type GTPases mediate KNOLLE internalization to restrict spreading of this syntaxin to lateral membranes of late cytokinetic cells in *Arabidopsis*. Hence, it will be interesting to see whether fungal and animal cells use similar or different mechanisms to control syntaxin localization during cytokinetic vesicle fusion.

Materials and methods

Plant material and growth conditions

The *Arabidopsis thaliana* ecotypes Landsberg *erecta* (L*er*), Columbia-0 (Col-0), Wassilewskija (WS) and the following mutants were used: *cpi1-1* and *cpi1-1/+;pPIN2:PIN2-EGFP* (Men *et al*, 2008), *knolle*$^{X37\text{-}2}$ (Lukowitz *et al*, 1996), *smt1*$^{cph\text{-}G213}$ (Schrick *et al*, 2002), *smt1*^{orc} (Willemsen *et al*, 2003), *drp1a*^{rsw9}, *drp1a*$^{SALK\_069077}$ (Collings *et al*, 2008). The SALK_069077 insertion line into the *DRP1A* locus (Alonso *et al*, 2003; Collings *et al*, 2008) was obtained through the Nottingham *Arabidopsis* Stock Centre with stock number N569077. The insertion was confirmed by PCR-based genotyping, using primers described in the Supplementary data. Molecular characterization of *cpi1-1; kn*$^{X37\text{-}2}$ and *drp1a*^{rsw9};*cpi1-1* double mutants was performed by PCR-based genotyping using primers

described in the Supplementary data. The following transgenic fluorescent-protein marker lines in Col-0 background were used: pRAB-A2a:YFP-RAB-A2a (Chow *et al*, 2008), pARF1:ARF1-EGFP, pHSP:ARF1-EGFP, pHSP:arf1-T31N-CFP (all fusions of AtARFA1c, At2g47170) (Xu and Scheres, 2005), pARA6:ARA6-GFP/pRAB-F1:RAB-F1-GFP (Goh *et al*, 2007), p35S:GFP-RAB-F2b (Jaillais *et al*, 2006), pVHA-a1:VHA-a1-GFP (Dettmer *et al*, 2006), p35S:*N*-ST-YFP and p35S:NAG1-EGFP (Grebe *et al*, 2003). The pKNOLLE:GFP-KNOLLE was in a L*er*/Niederzens (L*er*/Nd) background (Reichardt *et al*, 2007); pDRP1A:DRP1A-mGFP5 (Kang *et al*, 2003) and p35S:ER-mGFP5-HDEL from J. Haseloff (Grebe *et al*, 2003) were in WS background. Plant growth conditions were as described (Men *et al*, 2008). Analyses were carried out on 5-day-old seedlings. Seedlings from heat-shock-inducible lines (Xu and Scheres, 2005) were grown on agar plates for 5 days, transferred to 37°C for 90 min and placed back to 25°C for a recovery time of 4 h before analysis.

Inhibitor treatments

For inhibitor experiments, seedlings were treated in liquid medium (LM) containing 1 × Murashige and Skoog, 1% sucrose, 2.5 mM morpholinoethanesulfonic acid (Sigma) at pH 5.8. BFA (Sigma) dissolved in DMSO was used at 25 μM for 2 h, or 50 μM for 1 h. TyrA23 and TyrA51 (Sigma) dissolved in DMSO were used at 50 μM for 1 h. TyrA23 (50 μM, 1 h) wash-out experiments were performed by washing with LM containing DMSO at equal concentration to the inhibitor-treated samples. CHX was added from a 50 mM aqueous stock to a final concentration of 50 μM. Treatment of seedlings with 0.02% sodium azide and 50 mM 2-deoxy-D-glucose was as described (Men *et al*, 2008). The fen (PESTANAL, Sigma) was dissolved at 200 mg/ml in DMSO. For fen treatment, seedlings were grown on agar plates consisting of the above medium containing 0.8% plant agar (Duchefa) and 200 μg/ml fen for 5 days. Control plates contained an equal amount of 0.1% DMSO solvent.

Immunocytochemistry, FM4-64 staining and confocal laser-scanning microscopy

Whole-mount immunolabelling as well as fluorescence detection by confocal laser-scanning microscopy (CLSM), using a Leica TCS SP2 AOBS (Leica) spectral CLSM system mounted on an LEICA DM IRE2 inverted microscope were performed as described (Men *et al*, 2008). Antibodies dilutions were rabbit anti-KNOLLE, 1:4000 (Lauber *et al*, 1997); Cy5-coupled, donkey anti-rabbit IgG, 1:300 (Jackson ImmunoResearch). FM4-64 staining in the GFP-KNOLLE background was performed by incubating seedlings in LM in the presence of 25 μM of FM4-64 (Molecular Probes) (from a 10 mM stock in DMSO) for 5 min on ice. This was followed by two washes with LM on ice, mounting on coverslips in LM medium containing inhibitors as specified and subsequent observation by CLSM. Laser excitation lines for the different fluorophores were 364 nm for filipin–sterol, 405 nm for DAPI, 458, 488, 514 nm for CFP, GFP and YFP fluorescence, respectively, 561 nm for FM4-64 and 633 nm for Cy5 fluorescence. Fluorescence emission was detected at 400–484 nm for filipin–sterol, 410–484 nm for DAPI, 505–600 nm for CFP, 492–557 nm for GFP, 518–557 nm for YFP, 600–700 nm for FM4-64 and 637-750 nm for Cy5 fluorescence. In multi-labelling studies, detection was in sequential line-scanning mode with a line average of 8. An oil-corrected 63 × objective, NA = 1.4 (HCX PL APO 63.0 × 1.40 OI BD UV, Leica) was used in immuno- and filipin–sterol-labelling studies. A water-corrected 63 × objective, NA = 1.2 (HCX PL APO 63.0 × 1.20 W BD UV, Leica) was used for FM4-64 detection. Filipin–sterol staining of roots and fluorescence detection was as described (Grebe *et al*, 2003; Men *et al*, 2008). Pictures were overlaid in Adobe Photoshop CS2 and assembled in Adobe Illustrator CS2 (Adobe).

Filipin–sterol and immunofluorescence co-labelling

For filipin–sterol and anti-KNOLLE co-labelling, a two-step filipin-staining procedure (Grebe *et al*, 2003) was used with minor modifications. After filipin labelling, root tips were bisected and allowed to dry on poly-L-lysine slides (VWR international). Subsequently, the following minor modifications were introduced to optimize for KNOLLE-antibody labelling: 2% driselase was applied for 45 min rather than 30 min, and, during subsequent membrane permeabilization, DMSO was replaced by filipin III (Sigma) dissolved in DMSO at 1 mg/ml (from a stock solution of 10 mg/ml) and IGEPAL (Sigma) included at 3% (v/v).

FLIP and FRAP analyses

FLIP and FRAP analyses were performed after earlier established protocols (Grebe *et al*, 2003; Men *et al*, 2008), using the Leica CLSM described above and Leica TCS FRAP software. For a detailed description, see Supplementary data.

DRM analysis

DRM extraction was performed as described (Borner *et al*, 2005). In brief, 200 ml of *A. thaliana* root-cell suspension culture (Col-0) were grown for 3 days under a 16 h light/8 h dark cycle at 25°C. Cultures were harvested by centrifugation at 1600 *g* for 10 min, resuspended in two volumes of homogenization buffer and TM collected as described (Borner *et al*, 2005). Protein quantification was performed using a Bicinchoninic acid (BCA) protein assay kit (Termo Scientific). A total of 2.5 mg of TM protein were incubated with 0 (ratio 0), 10 mg (ratio 4) or 20 mg (ratio 8) of Triton-X-100 for 35 min on ice under agitation at 100 r.p.m. The final volume at different ratios was kept constant so that the percentage of Triton-X-100 did not exceed 3% at ratio 8. After sucrose-step-gradient centrifugation, DRMs were collected as described (Borner *et al*, 2005). DRM-protein concentration was determined using a BCA kit. Equal amounts of protein from different fractions or extractions were separated by SDS–PAGE and subjected to western blotting. The following antibodies and dilutions were used: rabbit anti-KNOLLE, 1:4000 (Lauber *et al*, 1997); mouse monoclonal anti-Hsc70 antibody, plant ER BiP, 1:1000 (Nordic Biosite AB); mouse monoclonal, anti-PM-H^+-ATPase, clone 46E5B11D5, 1:1000 (Langhans *et al*, 2001); rabbit anti-SMT1, 1:50 (see Supplementary data); goat anti-mouse IgG-HRP conjugate (1:3000, Bio-Rad); ECL donkey anti-rabbit IgG-HRP-linked whole Ab, 1:8000 (Amersham). An ECL western-blotting detection reagent kit (Amersham) was used for detection.

Quantitative fluorescence co-localization analyses and electron microscopy

Quantitative fluorescence co-localization analyses was performed as described earlier (Boutté *et al*, 2006) and electron microscopy of filipin–sterol complex localization was performed essentially as described (Grebe *et al*, 2003) with minor modifications, as explained in the Supplementary data section.

Supplementary data

Supplementary data are available at *The EMBO Journal* Online (http://www.embojournal.org).

Acknowledgements

We gratefully acknowledge S Bednarek, T Gaude, J Haseloff, W Michalke, B Scheres, K Schumacher, K Schrick and R Williamson for sharing published research materials that were important for this study. We also thank J Alonso and J Ecker for making available T-DNA insertion lines from the Salk collection and the Nottingham *Arabidopsis* Stock Centre for their distribution. Moreover, we thank R Bhalerao for helpful comments on the paper. This work was supported by a grant from the Swedish Research Council for Environment, Agricultural Sciences and Spatial Planning (Formas) to MG and a postdoctoral stipend from the Carl Tryggers Foundation to YB.

Conflict of interest

The authors declare that they have no conflict of interest.

References

Alonso JM, Stepanova AN, Leisse TJ, Kim CJ, Chen H, Shinn P, Stevenson DK, Zimmerman J, Barajas P, Cheuk R, Gadrinab C, Heller C, Jeske A, Koesema E, Meyers CC, Parker H, Prednis L, Ansari Y, Choy N, Deen H *et al* (2003) Genome-wide

insertional mutagenesis of *Arabidopsis thaliana*. *Science* **301:** 653–657

Barr FA, Grüneberg U (2007) Cytokinesis: placing and making the final cut. *Cell* **131:** 847–860

Borner GH, Sherrier DJ, Weimar T, Michaelson LV, Hawkins ND, Macaskill A, Napier JA, Beale MH, Lilley KS, Dupree P (2005) Analysis of detergent-resistant membranes in *Arabidopsis*. Evidence for plasma membrane lipid rafts. *Plant Physiol* **137:** 104–116

Boutté Y, Crosnier MT, Carraro N, Traas J, Satiat-Jeunemaitre B (2006) The plasma membrane recycling pathway and cell polarity in plants: studies on PIN proteins. *J Cell Sci* **119:** 1255–1265

Boutté Y, Grebe M (2009) Cellular processes relying on sterol function in plants. *Curr Opin Plant Biol* **12** (in press; doi:10.1016/j.pbi.2009.09.013)

Chow CM, Neto H, Foucart C, Moore I (2008) Rab-A2 and Rab-A3 GTPases define a trans-Golgi endosomal membrane domain in *Arabidopsis* that contributes substantially to the cell plate. *Plant Cell* **20:** 101–123

Collings DA, Gebbie LK, Howles PA, Hurley UA, Birch RJ, Cork AH, Hocart CH, Arioli T, Williamson RE (2008) *Arabidopsis* dynamin-like protein DRP1A: a null mutant with widespread defects in endocytosis, cellulose synthesis, cytokinesis, and cell expansion. *J Exp Bot* **59:** 361–376

Cutler SR, Ehrhardt DW (2002) Polarized cytokinesis in vacuolate cells of *Arabidopsis*. *Proc Natl Acad Sci USA* **99:** 2812–2817

Dettmer J, Hong-Hermesdorf A, Stierhof YD, Schumacher K (2006) Vacuolar H+-ATPase activity is required for endocytic and secretory trafficking in *Arabidopsis*. *Plant Cell* **18:** 715–730

Dhonukshe P, Aniento F, Hwang I, Robinson DG, Mravec J, Stierhof YD, Friml J (2007) Clathrin-mediated constitutive endocytosis of PIN auxin efflux carriers in *Arabidopsis*. *Curr Biol* **17:** 520–527

Dhonukshe P, Baluška F, Schlicht M, Hlavacka A, Šamaj J, Friml J, Gadella Jr TW (2006) Endocytosis of cell surface material mediates cell plate formation during plant cytokinesis. *Dev Cell* **10:** 137–150

Dhonukshe P, Tanaka H, Goh T, Ebine K, Mähönen AP, Prasad K, Blilou I, Geldner N, Xu J, Uemura T, Chory J, Ueda T, Nakano A, Scheres B, Friml J (2008) Generation of cell polarity in plants links endocytosis, auxin distribution and cell fate decisions. *Nature* **456:** 962–966

Fernandez C, Lobo Md Mdel V, Gomez-Coronado D, Lasuncion MA (2004) Cholesterol is essential for mitosis progression and its deficiency induces polyploid cell formation. *Exp Cell Res* **300:** 109–120

Geldner N, Anders N, Wolters H, Keicher J, Kornberger W, Muller P, Delbarre A, Ueda T, Nakano A, Jürgens G (2003) The *Arabidopsis* GNOM ARF-GEF mediates endosomal recycling, auxin transport, and auxin-dependent plant growth. *Cell* **112:** 219–230

Geldner N, Friml J, Stierhof YD, Jürgens G, Palme K (2001) Auxin transport inhibitors block PIN1 cycling and vesicle trafficking. *Nature* **413:** 425–428

Goh T, Uchida W, Arakawa S, Ito E, Dainobu T, Ebine K, Takeuchi M, Sato K, Ueda T, Nakano A (2007) VPS9a, the common activator for two distinct types of Rab5 GTPases, is essential for the development of *Arabidopsis thaliana*. *Plant Cell* **19:** 3504–3515

Grebe M, Xu J, Möbius W, Ueda T, Nakano A, Geuze HJ, Rook MB, Scheres B (2003) *Arabidopsis* sterol endocytosis involves actin-mediated trafficking via ARA6-positive early endosomes. *Curr Biol* **13:** 1378–1387

Gromley A, Yeaman C, Rosa J, Redick S, Chen CT, Mirabelle S, Guha M, Sillibourne J, Doxsey SJ (2005) Centriolin anchoring of exocyst and SNARE complexes at the midbody is required for secretory-vesicle-mediated abscission. *Cell* **123:** 75–87

He JX, Fujioka S, Li TC, Kang SG, Seto H, Takatsuto S, Yoshida S, Jang JC (2003) Sterols regulate development and gene expression in *Arabidopsis*. *Plant Physiol* **131:** 1258–1269

Jaillais Y, Fobis-Loisy I, Miege C, Rollin C, Gaude T (2006) AtSNX1 defines an endosome for auxin-carrier trafficking in *Arabidopsis*. *Nature* **443:** 106–109

Jantsch-Plunger V, Glotzer M (1999) Depletion of syntaxins in the early *Caenorhabditis elegans* embryo reveals a role for membrane fusion events in cytokinesis. *Curr Biol* **9:** 738–745

Jürgens G (2005) Cytokinesis in higher plants. *Annu Rev Plant Biol* **56:** 281–299

Kang BH, Busse JS, Bednarek SY (2003) Members of the *Arabidopsis* dynamin-like gene family, *ADL1*, are essential for plant cytokinesis and polarized cell growth. *Plant Cell* **15:** 899–913

Klemm RW, Ejsing CS, Surma MA, Kaiser HJ, Gerl MJ, Sampaio JL, de Robillard Q, Ferguson C, Proszynski TJ, Shevchenko A, Simons K (2009) Segregation of sphingolipids and sterols during formation of secretory vesicles at the trans-Golgi network. *J Cell Biol* **185:** 601–612

Konopka CA, Backues SK, Bednarek SY (2008) Dynamics of *Arabidopsis* dynamin-related protein 1C and a clathrin light chain at the plasma membrane. *Plant Cell* **20:** 1363–1380

Konopka CA, Bednarek SY (2008) Comparison of the dynamics and functional redundancy of the *Arabidopsis* dynamin-related isoforms DRP1A and DRP1C during plant development. *Plant Physiol* **147:** 1590–1602

Laloi M, Perret AM, Chatre L, Melser S, Cantrel C, Vaultier MN, Zachowski A, Bathany K, Schmitter JM, Vallet M, Lessire R, Hartmann MA, Moreau P (2007) Insights into the role of specific lipids in the formation and delivery of lipid microdomains to the plasma membrane of plant cells. *Plant Physiol* **143:** 461–472

Langhans M, Ratajczak R, Lützelschwab M, Michalke W, Wachter R, Fischer-Schliebs E, Ullrich CI (2001) Immunolocalization of plasma-membrane H+-ATPase and tonoplast-type pyrophosphatase in the plasma membrane of the sieve element-companion cell complex in the stem of *Ricinus communis L*. *Planta* **213:** 11–19

Lauber MH, Waizenegger I, Steinmann T, Schwarz H, Mayer U, Hwang I, Lukowitz W, Jürgens G (1997) The *Arabidopsis* KNOLLE protein is a cytokinesis-specific syntaxin. *J Cell Biol* **139:** 1485–1493

Low SH, Li X, Miura M, Kudo N, Quinones B, Weimbs T (2003) Syntaxin 2 and endobrevin are required for the terminal step of cytokinesis in mammalian cells. *Dev Cell* **4:** 753–759

Lukowitz W, Mayer U, Jürgens G (1996) Cytokinesis in the *Arabidopsis* embryo involves the syntaxin-related KNOLLE gene product. *Cell* **84:** 61–71

Men S, Boutté Y, Ikeda Y, Li X, Palme K, Stierhof YD, Hartmann MA, Moritz T, Grebe M (2008) Sterol-dependent endocytosis mediates post-cytokinetic acquisition of PIN2 auxin efflux carrier polarity. *Nat Cell Biol* **10:** 237–244

Miller RG (1984) The use and abuse of filipin to localize cholesterol in membranes. *Cell Biol Int Rep* **8:** 519–535

Möbius W, van Donselaar E, Ohno-Iwashita Y, Shimada Y, Heijnen HF, Slot JW, Geuze HJ (2003) Recycling compartments and the internal vesicles of multivesicular bodies harbor most of the cholesterol found in the endocytic pathway. *Traffic* **4:** 222–231

Mongrand S, Morel J, Laroche J, Claverol S, Carde JP, Hartmann MA, Bonneu M, Simon-Plas F, Lessire R, Bessoule JJ (2004) Lipid rafts in higher plant cells: purification and characterization of Triton X-100-insoluble microdomains from tobacco plasma membrane. *J Biol Chem* **279:** 36277–36286

Montagnac G, Echard A, Chavrier P (2008) Endocytic traffic in animal cell cytokinesis. *Curr Opin Cell Biol* **20:** 454–461

Müller I, Wagner W, Völker A, Schellmann S, Nacry P, Küttner F, Schwarz-Sommer Z, Mayer U, Jürgens G (2003) Syntaxin specificity of cytokinesis in *Arabidopsis*. *Nat Cell Biol* **5:** 531–534

Orci L, Montesano R, Meda P, Malaisse-Lagae F, Brown D, Perrelet A, Vassalli P (1981) Heterogeneous distribution of filipin-cholesterol complexes across the cisternae of the Golgi apparatus. *Proc Natl Acad Sci USA* **78:** 293–297

Ortiz-Zapater E, Soriano-Ortega E, Marcote MJ, Ortiz-Masia D, Aniento F (2006) Trafficking of the human transferrin receptor in plant cells: effects of tyrphostin A23 and brefeldin A. *Plant J* **48:** 757–770

Pichler H, Riezman H (2004) Where sterols are required for endocytosis. *Biochim Biophys Acta* **1666:** 51–61

Pike LJ (2006) Rafts defined: a report on the Keystone Symposium on lipid rafts and cell function. *J Lipid Res* **47:** 1597–1598

Reichardt I, Stierhof YD, Mayer U, Richter S, Schwarz H, Schumacher K, Jürgens G (2007) Plant cytokinesis requires *de novo* secretory trafficking but not endocytosis. *Curr Biol* **17:** 2047–2053

Samuels AL, Giddings Jr TH, Staehelin LA (1995) Cytokinesis in tobacco BY-2 and root tip cells: a new model of cell plate formation in higher plants. *J Cell Biol* **130:** 1345–1357

Schrick K, Fujioka S, Takatsuto S, Stierhof YD, Stransky H, Yoshida S, Jürgens G (2004) A link between sterol biosynthesis, the cell wall, and cellulose in *Arabidopsis*. *Plant J* **38:** 227–243

Schrick K, Mayer U, Horrichs A, Kuhnt C, Bellini C, Dangl J, Schmidt J, Jürgens G (2000) FACKEL is a sterol C-14 reductase required for organized cell division and expansion in *Arabidopsis* embryogenesis. *Genes Dev* **14:** 1471–1484

Schrick K, Mayer U, Martin G, Bellini C, Kuhnt C, Schmidt J, Jürgens G (2002) Interactions between sterol biosynthesis genes in embryonic development of *Arabidopsis*. *Plant J* **31:** 61–73

Simons K, Ikonen E (1997) Functional rafts in cell membranes. *Nature* **387:** 569–572

Ueda T, Yamaguchi M, Uchimiya H, Nakano A (2001) Ara6, a plant-unique novel type Rab GTPase, functions in the endocytic pathway of *Arabidopsis thaliana*. *EMBO J* **20:** 4730–4741

Van Damme D, Coutuer S, De Rycke R, Bouget FY, Inze D, Geelen D (2006) Somatic cytokinesis and pollen maturation in *Arabidopsis* depend on TPLATE, which has domains similar to coat proteins. *Plant Cell* **18:** 3502–3518

Waizenegger I, Lukowitz W, Assaad F, Schwarz H, Jürgens G, Mayer U (2000) The *Arabidopsis KNOLLE* and *KEULE* genes interact to promote vesicle fusion during cytokinesis. *Curr Biol* **10:** 1371–1374

Willemsen V, Friml J, Grebe M, van den Toorn A, Palme K, Scheres B (2003) Cell polarity and PIN protein positioning in *Arabidopsis* require STEROL METHYLTRANSFERASE1 function. *Plant Cell* **15:** 612–625

Xu H, Brill JA, Hsien J, McBride R, Boulianne GL, Trimble WS (2002) Syntaxin 5 is required for cytokinesis and spermatid differentiation in *Drosophila*. *Dev Biol* **251:** 294–306

Xu J, Scheres B (2005) Dissection of *Arabidopsis* ADP-RIBOSYLATION FACTOR 1 function in epidermal cell polarity. *Plant Cell* **17:** 525–536

Zappel NF, Panstruga R (2008) Heterogeneity and lateral compartmentalization of plant plasma membranes. *Curr Opin Plant Biol* **11:** 632–640

